Available online at www.sciencedirect.com
SCIENCE DIRECT®
Journal of Power Sources 144 (2005) 473–485
JOURNAL OF POWER SOURCES
www.elsevier.com/locate/jpowsour

New developments on valve-regulated lead–acid batteries for advanced automotive electrical systems

M.L. Soria*, J.C. Hernández, J. Valenciano, A. Sánchez, F. Trinidad

Exide Technologies, Research and Innovation, Autovía A-2, km 42, E-19200 Azuqueca de Henares, Spain

Available online 25 December 2004

Abstract

The development of novel electrical systems for low emission vehicles demands batteries with specific cycling performance, especially under partial state of charge (PSOC) conditions. Moreover, according to the powertrain design, battery high power capability is demanded or this function can be assumed by a supercapacitor or a flywheel. This paper deals with the development of AGM and gel valve-regulated lead–acid batteries for advanced automotive applications.

AGM VRLA battery development was based on previous work for short autonomy high power UPS applications and on active material formulations with specific additives to improve battery life under high rate partial state of charge cycling conditions. The 18 Ah batteries showed excellent high rate capability (9 kW 10 s discharge peaks and 4 kW 5 s regenerative charge acceptance at 60% state of charge) and 110,000 power assist microcycles at 60% SOC and 2.5% DOD were fulfilled.

Moreover, as preliminary work in the development of a cost-effective and reliable gel battery to be used in combination of a supercapacitor in a 42 V mild-hybrid powertrain, VRLA batteries with conventional gel formulations have been tested according to novel automotive cycling profiles, mainly moderate cycling under partial state of charge conditions and simulating load management in a stop and start working profile.

Keywords: Valve-regulated lead–acid batteries; Hybrid vehicles; Cycle life; Failure mode analysis

1. Introduction

There is a growing concern among car manufacturers worldwide to develop vehicles with reduced fuel consumption and emissions to meet the requirements of the Kyoto Protocol [1]. The European Commission has adopted several policies based on agreements with industry such as the ACEA-EU agreement on average CO_2 emissions of new cars sold in the EU [2].

The "well-to-wheels analysis of future automotive fuels and powertrains in the European context" performed by EUCAR, CONCAWE and JRC [3] presents an exhaustive evaluation of the energy use and green house gas (GHG) emissions for a wide range of potential future fuel and powertrain options. Among the different solutions presented, hybrid technologies are considered both in the short term, with conventional engines, and also in the long term in hybrid CNG (compressed natural gas) vehicles, and fuel cell vehicles.

Since the launch of Toyota Prius in 1997, Japanese car manufacturers have focused their efforts mainly in high voltage vehicles (144–288 V) equipped with high power and low capacity Ni-MH batteries, mainly for vehicle boosting and to recuperate braking energy. In 2004, several American and Japanese car manufactures have announced the launch of hybrid sport utility vehicles (SUVs) with significant emission reductions [4], when compared to conventional models, due to the high fuel consumption levels of the latter. In Europe, development programmes are mainly focused on mild hybrid vehicles, in which novel electrical functions (such as stop and start, boosting and regenerative braking) and hybrid architectures will allow for a 10–20% fuel saving and emission reduction.

* Corresponding author. Tel.: +34 949 263 316; fax: +34 949 262 560.
E-mail addresses: soriaml@tudor.es (M.L. Soria), hernandezc@tudor.es (J.C. Hernández), valencianoj@tudor.es (J. Valenciano), trinidadf@tudor.es (F. Trinidad).

0378-7753/$ – see front matter © 2004 Elsevier B.V. All rights reserved.
doi:10.1016/j.jpowsour.2004.11.005

Nowadays, batteries represent the main solution to energy storage needs in a widespread number of autonomous applications, from vehicles and portable devices to isolated renewable systems (RES), through a variety of industrial uses, mainly related to assuring energy supply in case of mains failure (for example, UPS or telecommunications) [5]. However, novel vehicle concepts, now under development to comply with the stringent demands of lower fuel consumption and CO_2 emission reduction, require low cost and long life energy storage systems under new operating conditions, which demand simultaneously a high power capability as well as increased life performance. Moreover, the automotive market requirements for system reliability make it necessary to consider the electrical system as a whole, including the hardware and software required to provide efficient energy management [6].

No battery system alone can be considered up to date a solution, in terms of energy/power performance, life and cost goals, industrial development and recycling facilities, to cope with the stringent performance and cost demands of car manufacturers. According to the vehicle requirements (powertrain architecture and hybridisation degree) one or another storage technology could meet the specific performance requirements. Moreover, hybrid energy storage systems can also be considered in order to optimise each component performance thus leading to synergic cost reductions. Based on well-known valve-regulated lead–acid (VRLA) technologies, it is possible to adapt product characteristics to the vehicle specifications. However, cycling profile and calendar life requirements and cost limitations demand further research work to improve battery life and reliability.

Novel vehicle functions demand at the same time energy storage (to support electrical consumers during stops in stop and start functions) and also high power capability for vehicle start and to recuperate energy during braking. Power capability and cycle life are currently difficult to achieve together. For this reason, experimental work on VRLA batteries has been focused on two different directions, aimed at the development of high power AGM batteries with adequate life performance adapted to high rate partial state of charge (PSOC) applications and on the other hand, of moderate power, long life gel batteries for hybrid energy storage systems, in which an electrochemical double layer capacitor (supercapacitor) fulfils the vehicle peak power requirements and stores the energy recuperated during braking.

2. Experimental

The 12 V AGM prototype batteries have been assembled with standard ABS containers sized 180 mm × 75 mm × 150 mm, which are commonly used in the manufacture of 15 Ah gel VRLA batteries for stand-by applications. Positive and negative plates were prepared in a standard continuous manufacturing line, cured under standard conditions and then they were cut to size and stacked manually. A manual cast-on-strap (COS) tooling was used to weld together the plate lugs and finally the ABS case and cover, and the valve plugs were welded with a laboratory ultrasound device.

The battery design was based on former work on the development of high power VRLA batteries for UPS applications [7,8], and was characterised by thin plate technology (around 1 mm thickness) and the use as separator of a combination of absorptive glass mat (AGM) material (supplied by Bernard Dumas S.A., FR) and a microporous polyethylene membrane (supplied by Daramic Inc., DE) to avoid premature battery failure due to short circuits. Based on previous work on active material formulations for hybrid vehicle applications [9,10], prototype batches with different negative active material formulations were assembled and tested to check their performance according to specific procedures for hybrid vehicles and 42 V vehicle applications.

Moreover, a batch of gel prototypes was assembled using standard polypropylene containers sized 175 mm × 80 mm × 174 mm (motorcycle type), plates prepared with standard gravity casted grids and SLI standard positive and negative active material formulations and Darak 2000 leaf separators (Daramic, DE). Gel electrolyte was prepared mixing a solution of sulphuric acid with 6% fumed silica (Aerosil 200, Degussa, DE), using a high-speed stirrer.

Electrical testing of the batteries was carried out with computer controlled cycling equipment: Bitrode LCN-7-100-12 and Digatron UBT 100-60-3 BTS and HEW 2000/12-700/36. High rate discharges were performed with a computer controlled Digatron UBT BTS-500, model HEW 2000-6BTS. After the initial tests, the AGM batteries were submitted to selected tests included in the specifications developed by EUCAR Traction Battery Working Group for hybrid vehicle and for 42 V applications (December 1998 and August 2003, respectively) [11] and other battery specifications, mainly discharges at different rates, determination of high power capability and charge acceptance at different states of charge, rates and temperatures and cycle life testing at moderate and high rate and partial state of charge conditions (PSOC). A tear-down analysis of the batteries was finally performed to establish the failure mode.

Tests of gel batteries included initial capacity check at different rates, cold cranking and cycle life performance under different partial state of charge conditions, mainly simulating moderate rate charge and discharge working profiles.

Chemical analysis of the active material samples were carried out using internal procedures based on volumetric (PbO_2) and gravimetric ($PbSO_4$) procedures. Active material porosity was measured with a mercury intrusion porosimeter Micromeritics Autopore 9405 and specific surface (BET) with a Micromeritics FlowSorb II 2300. Morphological studies have been carried out by scanning electron microscopy.

Table 1
Battery design characteristics

	Group A	Group B	Group C	Group D
Positive plates				
Paste density (g cm^{-3})	4.2	4.3	4.2	4.0
Active material weight (g plate^{-1})	29	28	29	29
Negative plates				
Paste density (g cm^{-3})	4.5	4.3	4.3	4.2
Active material weight (g plate^{-1})	26	30	30	29
Vanisperse A (%)	0.3	0.2	0.2	0.2
Expanded graphite (%)	–	1.5	1.5	1.5
Carbon black (%)	0.2	–	–	–
Separator type	AGM + PE membrane	AGM	AGM + PE membrane	AGM + PE membrane
Battery weight (kg)	6.4	6.4	6.5	6.4

3. Results and discussion

3.1. AGM high power batteries

3.1.1. Prototype characteristics and initial capacity check

Table 1 shows the design characteristics of the four groups of batteries tested. Prototypes were assembled with thin electrodes (around 1 mm thickness) and each cell contained eight positive and seven negative electrodes. Group A, selected as control batteries, contained standard negative active material formulation with 0.3% Vanisperse A (Borregaard, SE) as expander and 0.2% carbon black (Lamp black 100, Degussa, DE). The other prototype groups were manufactured including a higher content of carbon compound in the negative mass formulation (1.5% of expanded graphite material, Superior Graphite ABG1010, characterised by a specific surface of 24 m^2 g^{-1}), as well as a lower expander amount (0.2% Vanisperse A), according to previous studies [10], to improve battery charge acceptance characteristics.

As shown in Table 1, positive active material formulation was similar for all the groups (4.2–4.3 g cm^{-3}) except for type D prototypes, in which a lower positive paste density was used (4.0 g cm^{-3}). Group B prototypes were manufactured with only AGM separator whereas groups A, C and D were assembled including a three-layer separator configuration: a strip of polyethylene membrane (0.14 mm thickness) sandwiched between two 0.5 mm thick AGM layers [8].

First, the prototypes were electrically characterised, the results being summarised in Table 2. As shown, prototype capacity ranged from 18.1 to 18.9 Ah, at the 20 h rate, and all prototype groups showed excellent high power performance at low temperature: cold cranking at −18 °C and 300 A (over 15*C* rate) ranged between 34 and 39 s. Electrical resistance was measured with an AC Milliohmeter after prototype preliminary testing and ranged between 5.5 and 5.8 mΩ.

3.1.2. Constant current discharges

To establish the discharge performance at different rates, prototypes from groups A and D, with standard and optimised negative active material formulations, respectively, were discharged to 9.0 V under constant current conditions at the following rates: 0.9, 7.5, 15, 30, 75, 150 and 225 A. Fig. 1 shows a diagram in which the discharge current versus discharge duration are represented in a logarithm scale, and also the linear regressions of the values obtained (Peukert curves), that allow to estimate the battery performance under any other discharge conditions. Similar values for a standard AGM battery have been included for comparison purposes. The figure shows the quite similar performance of both types of UHP prototypes, and how the Peukert curve for the standard AGM batteries diverges from the UHP ones, when higher discharge rates are considered.

Regression coefficients have been used to calculate the *n* and *K* constants of the empirical Peukert equation: $I^n t = K$. In this way, similar n constants were obtained for UHP prototypes A and D ($n = 1.19$ in both cases) and a higher value for standard AGM batteries ($n = 1.29$), which indicates a better utilisation of active materials in UHP prototypes, as *n* approaches unity [12]. *K* figures obtained were 23.8, 23.4 and 19.3 for UHP prototypes A and D and standard AGM batteries, respectively.

Table 2
Electrical testing of batteries with different negative active material formulations

	Testing conditions	Group A	Group B	Group C	Group D
Capacity (Ah)					
C_{20}	0.9 A, 10.5 V, 25 °C	18.5	18.9	18.3	18.1
C_1	15 A, 9.6 V, 25 °C	15.2	15.6	14.7	15.6
Reserve capacity (min)	25 A, 10.5 V, 25 °C	28.2	30.2	25.8	31.2
Cold cranking (s)	300 A, −18 °C, 7.2 V	34	36	34	39
Internal resistance (mΩ)	1 kHz, 25 °C	5.8	5.6	5.5	5.6

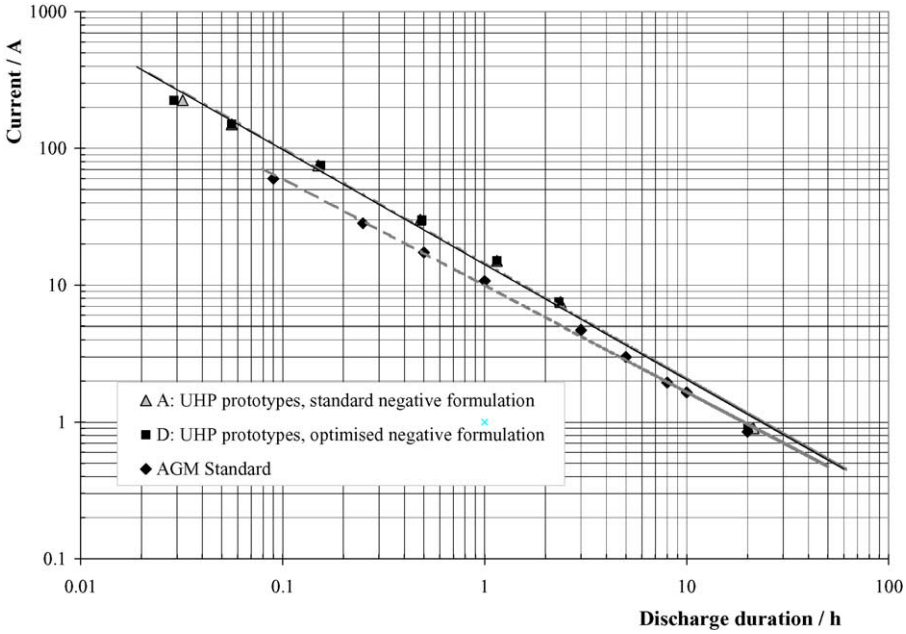

Fig. 1. Peukert curves of UHP prototypes and standard AGM batteries.

3.1.3. High rate charge and discharge performance at room temperature

High power capability and high rate charge acceptance are important battery features in future hybrid vehicle concepts, as battery is aimed at assisting conventional engines during vehicle acceleration and to store energy from regenerative braking. The peak power and charge acceptance of 36 V UHP prototypes (three 12 V modules in series) have been tested at 25 °C and at different states of charge (SOC), ranging from 100 to 20%. Test conditions and results are summarised in Table 3. The peak power values were obtained at 400 A, discharging down to 30 V and in the charge acceptance test the maximum voltage was limited to 48 V (2.65 V cell^{-1}). If a lower charging voltage value is considered (i.e. 45 V or 2.5 V cell^{-1}) charge acceptance decreases, specially at low states of charge, however, this could improve battery life, due to the fact that excessive gassing might be detrimental in case of prolonged high rate charging conditions.

As shown in Table 3, UHP prototypes of type D show lower discharge power values (around 10–15%) than type A, whereas their charge acceptance at low states of charge (under 60% SOC) is moderately higher (10–15%). As expected, average charge acceptance decreased significantly when charge duration increased from 5 to 10 s. In any case, the best compromise between peak power and charge acceptance values corresponds to around 60% SOC: for the 36 V UHP A prototype, nearly 9 kW in a 10 s discharge down to 30 V and over 4 kW in 5 s regenerative charge acceptance at 45 V were obtained.

Moreover, Fig. 2 shows open circuit voltage measured at different state of charge conditions as well as the internal resistance values calculated according to the EUCAR test procedures, based on initial ohmic drops during discharges at different rates. Open circuit voltage decreases from 39.6 to 36.2 V (2.2–2.0 V cell^{-1}) when the battery is discharged to 20% SOC whereas the internal resistance increases around one third in the same conditions.

3.1.4. Power capability at low temperature

Peak power capability of UHP prototypes A and D has also been tested at −30 °C. The 36 V batteries were discharged at 400 A/21 V during 10 s at full charge and 80% SOC. Results obtained are shown in Table 4. Up to 8 kW

Table 3
Peak power capability and charge acceptance at 25 °C of 36 V UHP prototypes (A: standard negative formulation/D: optimised negative formulation)

	Conditions	State of charge (%)				
		100	80	60	40	20
36 V UHP A						
Discharge power (W kg^{-1})						
1 s peak	400 A, 30 V	593	577	526	438	335
Average 10 s	400 A, 30 V	552	510	443	371	278
Charge acceptance (W kg^{-1})						
1 s peak	300 A, 48 V	–	134	258	392	490
Average 5 s	300 A, 48 V	–	125	227	325	423
Average 5 s	300 A, 45 V	–	123	211	304	376
36 V UHP D						
Discharge power (W kg^{-1})						
1 s peak	400 A, 30 V	501	509	448	381	325
Average 10 s	400 A, 30 V	485	448	387	325	273
Average 30 s	400 A, 24 V	557	515	412	294	196
Charge acceptance (W kg^{-1})						
1 s peak	300 A, 48 V	–	124	278	423	474
Average 5 s	300 A, 48 V	–	114	247	371	448
Average 10 s	300 A, 48 V	–	67	119	186	299

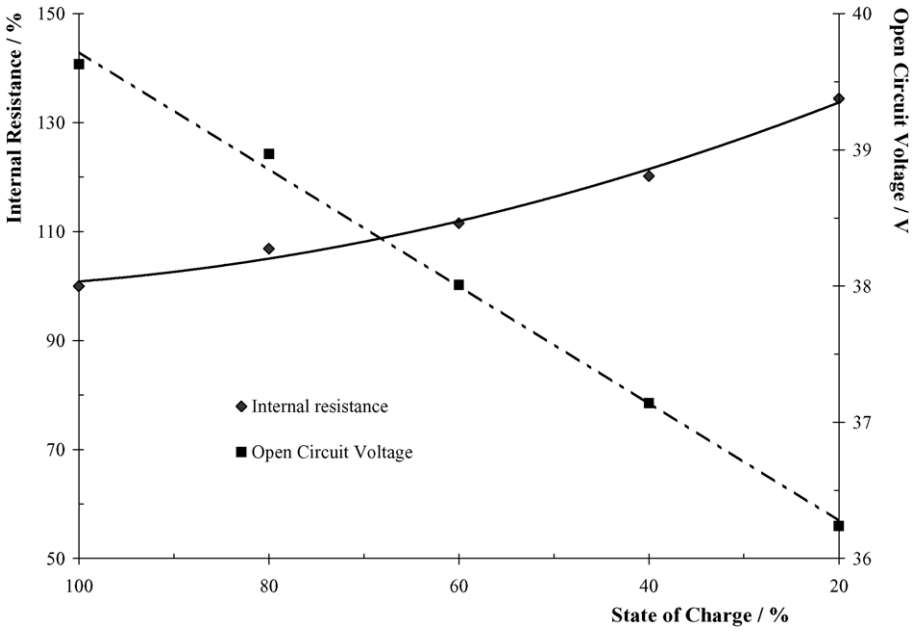

Fig. 2. Open circuit voltage and internal resistance of UHP D prototypes at different states of charge.

(412 W kg^{-1}) could be obtained as average power during 10 s with the batteries completely charged, and decreased to 4.5–5 kW (230–260 W kg^{-1}) at 80% SOC. At lower states of charge, power capability decreases strongly due to initial ohmic voltage drop. These values are higher than those reported for advanced batteries at such a low temperature: around 150 W kg^{-1} at −30 °C for the new Ni-MH battery modules developed for hybrid vehicles [16].

3.1.5. Power assist cycle life test and failure mode analysis

To check the performance of the batteries under high rate partial state of charge conditions (EUCAR power assist cycle life test [11]), 12 V prototype modules were discharged to 60% SOC and then cycled according to the microcycle profile shown in Fig. 3. Two discharge currents were selected, that is, 100 A (as shown in Fig. 3, UHP B prototypes) and 75 A (5*C*) adjusting the recharge coefficient to 101–102% (UHP prototypes A and C). The batteries were refrigerated with forced air (25 °C) to avoid an excessive temperature increase. Every 10,000 cycles a control capacity test and a complete charge were carried out.

Fig. 4 shows the end of discharge voltage evolution of UHP prototypes along the power assist cycling test. Type B prototypes, even including graphite in negative plates, have fulfilled only 40,000 cycles with a remaining capacity below 20% of the initial. The moderate cycle performance can be thus attributed to the high discharge demand (100 A, 3.3% DOD) of this particular profile. When the discharge rate was reduced to 75 A (5*C*, 2.5% DOD), and the recharge coefficient adjusted to 102%, UHP prototypes type A with standard negative formulation (0.3% Vanisperse A as expander and 0.2% carbon black) failed after 40,000–60,000 cycles due to voltage drop under 10 V during cycling, whereas UHP prototypes type C, with 0.2% Vanisperse and 1.5% expanded graphite in the negative active material, completed 80,000–110,000 cycles, as shown in Fig. 4. Besides longer life, prototypes containing graphite showed significantly higher end of discharge voltage values along life. This behaviour could be attributed to both the higher surface area and conductivity provided by the new carbon material that allows for a better rechargeability of graphite prototypes under high rate partial state of charge cycling conditions.

Moreover, battery AC internal resistance was measured every 10,000 microcycles and its evolution along power assist cycling is shown in Fig. 5, indicated as percentage increase, for the three types of prototypes tested. The highest increase corresponds to the group B, which, even though negative plates contained graphite, was tested at the highest depth of discharge ratio (3.3%). Comparing group A, with standard negative active material formulation, and group C, with 1.5% expanded graphite in the negative paste, it is clearly shown that the improvement in life and the higher end of discharge voltage during cycling (shown in Fig. 4) are due to a more steady increase in the internal resistance, and that the specific type of expanded graphite used improves active material conductivity along life.

Table 4
Discharge power of UHP prototypes at −30 °C (21 V, 400 A)

Discharge power (W kg^{-1})	UHP prototypes type A		UHP prototypes type D	
	100% SOC	80% SOC	100% SOC	80% SOC
1 s peak	454	345	459	371
10 s average	412	263	418	232

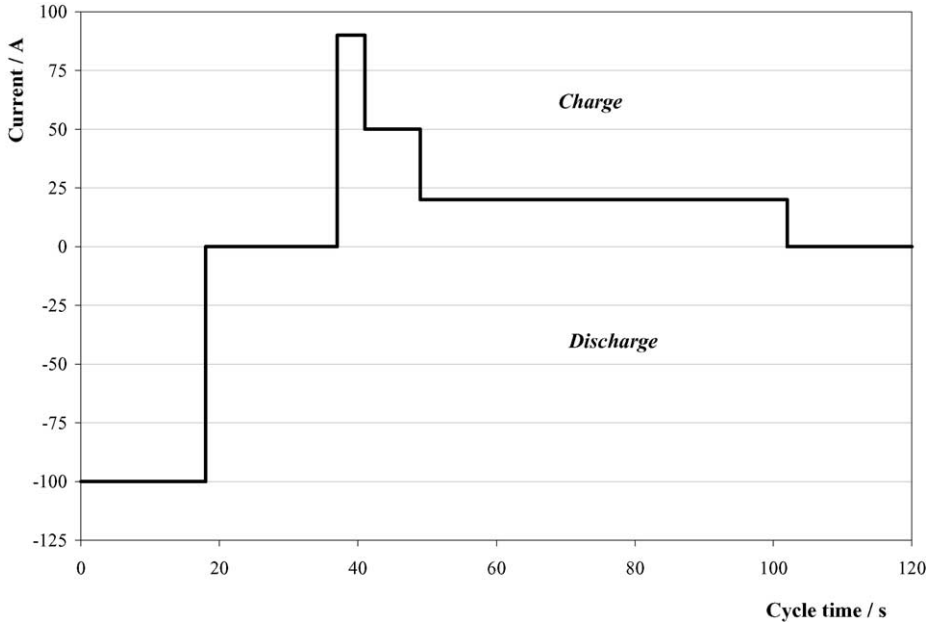

Fig. 3. EUCAR power assist microcycle profile.

Batteries were torn down and positive and negative plates were analysed to establish the battery failure modes. Analysis results are included in Table 5 and show a significantly high amount of sulphate in the negative active mass, even though positive plates contained very high PbO_2 levels (>90%). Therefore the main failure mode of the three groups of prototypes was a progressive and irreversible sulphation of the negative plates, mainly in the upper part of the electrodes. This fact provoked the increase of internal resistance measured along the cycling. The improved performance of batteries with graphite is clearly linked to a lower lead sulphate formation rate: after 110,000 microcycles, only 48.0% was detected in the upper part of electrodes from prototypes UHP C, compared to 79.6% in the same region of negatives electrodes with standard formulation (UHP A) after only 60,000 cycles. Lead sulphate formation rate is also increased by the higher depth of discharge: after 40,000 cycles at 3.3% DOD, UHP B prototypes showed 53% lead sulphate content. BET specific surface of negative electrodes decreases during cycling from 0.8 to 0.3–0.4 $m^2\,g^{-1}$ in the

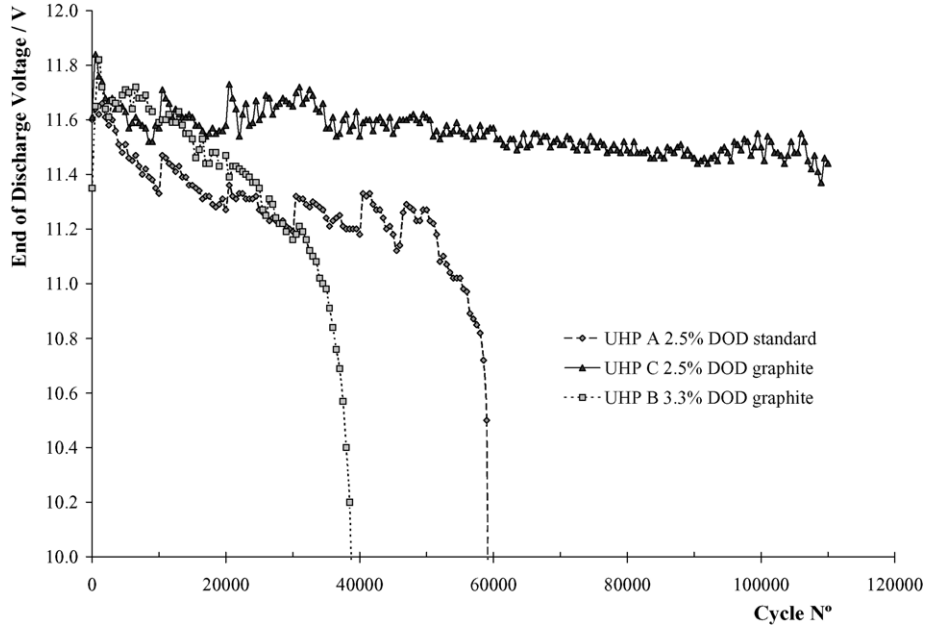

Fig. 4. End of discharge voltage evolution along the power assist cycle life test.

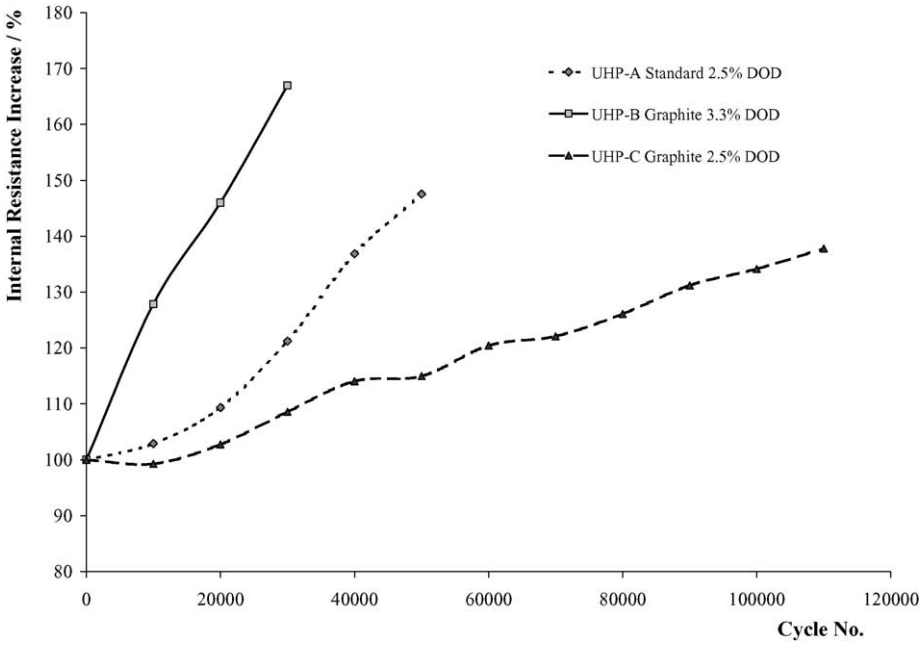

Fig. 5. Evolution of internal resistance of UHP prototypes along power assist cycle life.

upper part of the electrodes and 0.4–0.6 $m^2\ g^{-1}$ in the lower part.

Concerning positive plates, they showed good external appearance during tear-down visual inspection, and physico-chemical analysis of the active material showed, besides high PbO_2 contents, over 90%, a moderate porosity increase (around 10%), when compared to values obtained after battery formation, and a remarkable specific surface decrease during cycling: from 3.7–3.9 to 1.2–1.8 $m^2\ g^{-1}$.

An irreversible and selective sulphation of negative plates as main failure mode in AGM batteries subjected to high rate partial state of charge cycling profiles has also been described by Lam et al. [13], who observed, during cycling with a specific 42 V profile, a progressive accumulation of lead sulphate mainly on the surface of the negative electrodes, due to selective discharge of the external lead particles during short high rate discharges, that could not be later recharged under high rate conditions due to early hydrogen evolution provoked by a heavy polarisation of the negative electrode surface. However, with the EUCAR power assist profile and as reported previously by our group [14], lead sulphate was mainly accumulated in the upper part of the negative electrodes and SEM micrographs included in Figs. 6 and 7 show the clear morphological difference between the external and internal parts of the electrodes in the upper and lower areas: on the surface of the upper part (Fig. 6a and c), large lead sulphate polyhedral crystals can be observed, sized 2–10 μm, whereas the internal particles resemble the globular lead structure (in case of UHP C, Fig. 6d, with lower sulphation level due to graphite addition). In the lower part of the electrode (Fig. 7), small lead sulphate polyhedral crystals are mixed with globular lead particles. Presumably, during the high rate discharge step, formation of lead sulphate takes place mainly in the upper part of the electrode, which is the electrode area working during the 2.5 or 3.3% DOD discharge. During high rate charge, lead sulphate crystals cannot be recharged, and therefore, irreversible hard sulphate is progressively formed in the upper part of the electrodes, and mainly on the electrode surface.

Table 5
Tear-down analysis after power assist test (high rate and 60% SOC)

Prototype	Status	Positive active material analysis			Negative active material analysis[a]	
		PbO_2 (%)	Porosity (%)	BET ($m^2\ g^{-1}$)	$PbSO_4$ (%)	BET ($m^2\ g^{-1}$)
UHP A, standard negative formulation	After formation	87.9	48.9	3.71	4.9	0.81
	60,000 cycles, 2.5% DOD	96.4	54.1	1.2	79.6 (T), 7.4 (B)	0.29 (T), 0.38 (B)
UHP B, 1.5% expanded graphite in negative formulation	After formation	86.7	48.2	3.9	3.2	0.83
	40,000 cycles, 3.3% DOD	89.2	53.5	1.8	53.0 (T), 1.1 (B)	0.44 (T), 0.60 (B)
UHP C, 1.5% expanded graphite in negative formulation	After formation	87.9	48.7	3.70	2.6	0.80
	110,000 cycles, 2.5% DOD	93.2	52.1	1.21	48.0 (T), 15.5 (B)	0.35 (T), 0.43 (B)

[a] T: top, upper part of the plate; B: bottom, lower part of the plate.

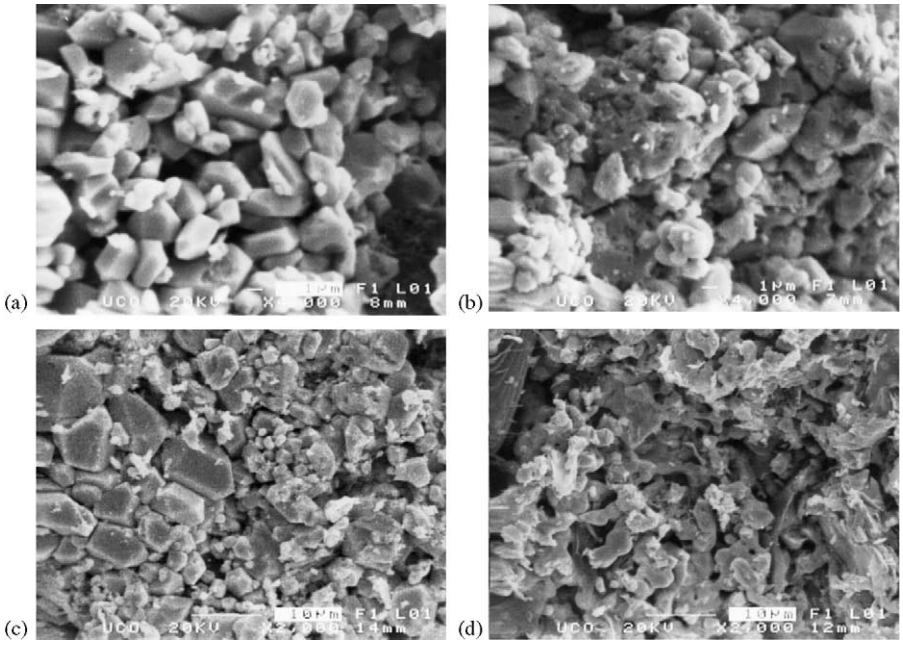

Fig. 6. Morphology of negative active material after power assist cycle life test (upper part of the electrodes): (a) UHP A after 60,000 microcycles, surface; (b) UHP A after 60,000 microcycles, inner region; (c) UHP C after 110,000 microcycles, surface; (d) UHP C after 110,000 microcycles, inner region.

3.1.6. Low rate partial state of charge cycle life

Finally, UHP A prototypes were tested according to a low–moderate rate (*C*/3) partial state of charge cycling, at 50% SOC and 17.5% DOD. Capacity check of the batteries every 85 cycles showed a steady capacity decrease along nearly 3000 cycles and finally the discharge voltage fell under 10 V, which was the test cut-off criterion. The results of the physico-chemical analysis of positive and negative active materials are indicated in Table 6, compared to the results obtained with active materials from the same type of batteries (UHP A) and after cycle life test at 60% DOD according to IEC 60896.2 [8] and at high rate partial state of charge (power assist), described previously in Section 3.1.5.

The results clearly show the different failure modes observed for the different cycling profiles. Batteries tested according to the low rate deep cycle life profile described in IEC 60896.2 (60% DOD, *C*/10 rate) failed due to ageing of the positive active material, which losses contacts between particles, as extensively described in the literature [15]. This fact is shown by the high porosity increase observed in the positive active material, from 48.9 to 61.4%, linked to a slight reduction of the specific surface, from 3.7 to 3.1 $m^2\ g^{-1}$. However, negative plates show a moderate sulphation of the negative electrodes, mainly in the lower part, due to the electrolyte stratification phenomenon (20% lead sulphate in the lower part, compared to 3.4% in the upper part of the plates).

In batteries subjected to partial state of charge and low–moderate rate cycling (50% SOC, 17.5% DOD, *C*/3 rate), failure mode can be ascribed mainly to positive active material degradation (58.2% porosity versus 48.9% after battery formation), although lead sulphate content in the negative active material, mainly in the lower part of the electrodes, is higher than in the deep cycle test: 38.5% versus 20.0%, respectively.

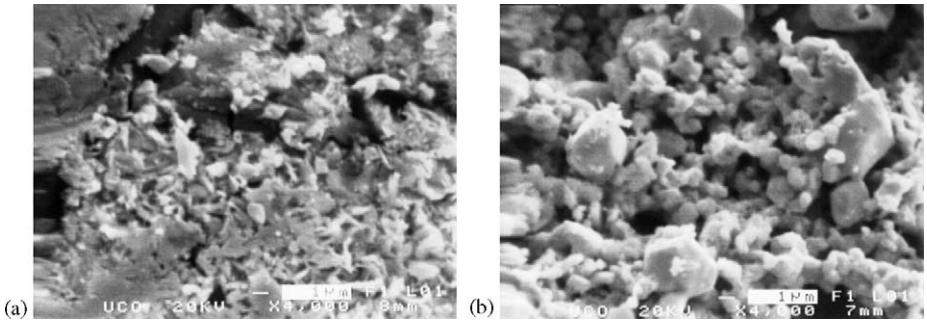

Fig. 7. Morphology of negative active material after power assist cycle life test (lower part of the electrodes): (a) UHP A after 60,000 microcycles, surface; (b) UHP A after 60,000 microcycles, inner region.

Table 6
Analysis of active materials from UHP A prototypes after formation and aged according to different cycle life conditions

Sample status	Positive active material analysis			Negative active material analysis[a]	
	PbO_2 (%)	Porosity (%)	BET ($m^2\ g^{-1}$)	$PbSO_4$ (%)	BET ($m^2\ g^{-1}$)
After formation	87.9	48.9	3.71	4.9	0.81
After 60,000 cycles, 2.5% DOD, 60% SOC	96.4	54.1	1.2	79.6 (T), 7.4 (B)	0.29 (T), 0.38 (B)
After 2975 cycles, 17.5% DOD, 50% SOC	94.5	58.2	2.65	4.2 (T), 38.5 (B)	0.35 (T), 0.36 (B)
After 400 cycles, 60% DOD, IEC 60896.2	82.6	61.4	3.1	3.4 (T), 20.0 (B)	0.36 (T), 0.32 (B)

[a] T: top, upper part of the plate; B: bottom, lower part of the plate.

Finally, as described previously in Section 3.1.5, batteries tested according to a high rate partial state of charge cycling profile (60% SOC, 2.5% DOD, 5*C* rate), failed due to a quite different mode, that is sulphation of the negative active material, predominantly in the upper part and surface of the plates, whereas the positive active mass was still healthy (high PbO_2 content, although lower BET surface area).

Fig. 8 shows the micrographs obtained by SEM from samples of positive active material from UHP prototypes type A after formation, after 400 cycles at *C*/10 rate and 60% DOD, after 2975 cycles at *C*/3 rate, 50% SOC and 17.5% DOD and after 60,000 cycles at 5*C* rate, 60% SOC and 2.5% DOD. The main difference is the size of the rounded PbO_2 particles, smaller (0.2–0.5 μm) in case of deep cycling conditions (60% DOD) and around 1–2 μm in the other cases.

The morphology of negative active material after formation and subjected to different cycling profiles can be observed in the photographs of Fig. 9. Lead particles show a globular structure with "melted" appearance, whereas in the lower part of the electrodes subjected to 17.5% DOD cycle life test, lead sulphate polyhedral crystals are clearly differentiated from globular lead particles, as shown in Fig. 9d.

Considering the three ageing conditions described previously, it can be concluded that, the higher the discharge depth, the higher porosity increase in the positive active material, which finally leads to a loss of the electroactive positive material structure (PbO_2 content >80%). When the battery is cycled under partial state of charge conditions, active material ageing depends strongly on the discharge/charge rate: low–moderate rates (*C*/3) led to similar degradation procedures in the positive electrodes than those found in deep cycling, whereas sulphation of negative electrodes is heavier, and mainly in the lower part. At high rate charge/discharge conditions, positive active material shows a lower porosity increase, whereas specific surface decreases strongly. However, negative electrodes are strongly sulphated and mainly in the upper part and on the surface. Moreover, in all cases studied, the specific surface of the negative electrodes was reduced to one half that measured after battery formation, due to the progressive loss of expander activity and sulphation.

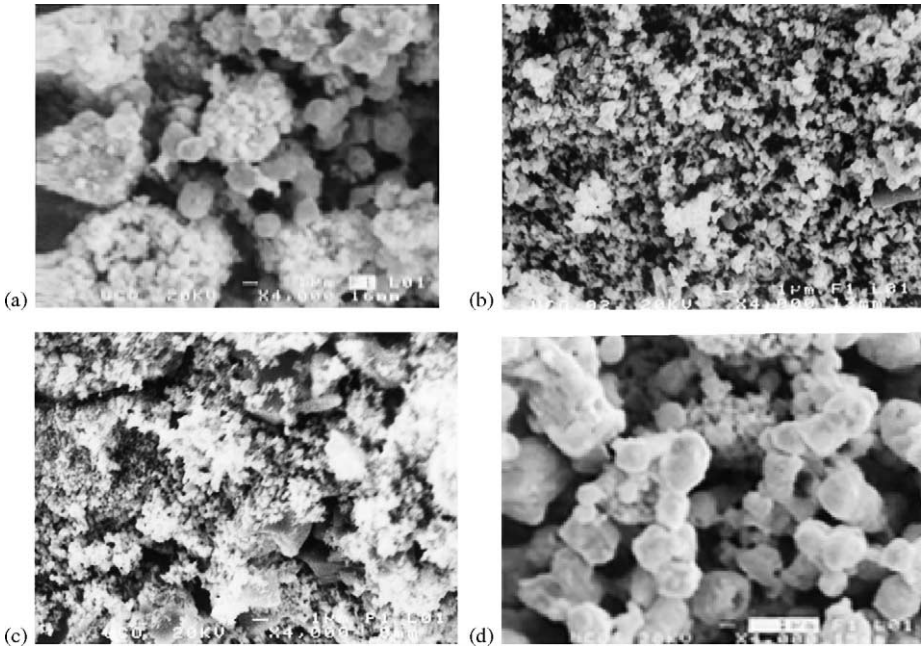

Fig. 8. SEM micrographs of positive active material from UHP A prototypes with different ageing conditions: (a) after battery formation; (b) after 400 cycles at *C*/10 rate and 60% DOD; (c) after 2975 cycles at *C*/3 rate, 50% SOC and 17.5% DOD; (d) after 60,000 microcycles at 5*C* rate, 60% SOC and 2.5% DOD.

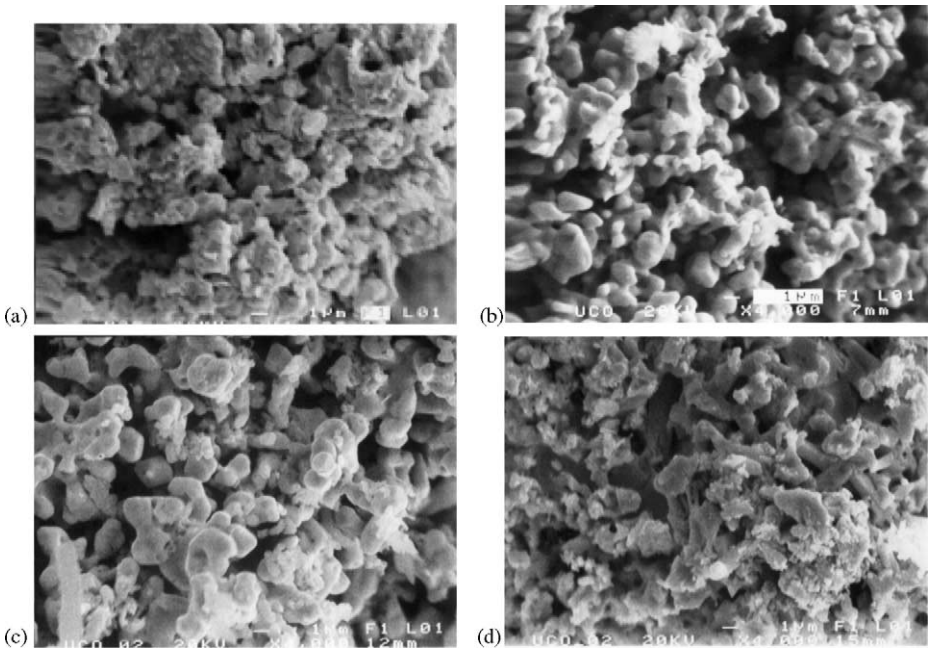

Fig. 9. SEM micrographs of negative active material from UHP A prototypes with different ageing conditions: (a) after battery formation; (b) after 400 cycles at *C*/10 rate and 60% DOD; (c) upper part after 2975 cycles at *C*/3 rate, 50% SOC and 17.5% DOD; (d) lower part after 2975 cycles at *C*/3 rate, 50% SOC and 17.5% DOD.

3.2. Gel batteries for automotive applications

Due to higher internal resistance (poorer cold cranking) and higher manufacturing costs, gel batteries are not commonly used in automotive applications. Only exceptions are motorcycle batteries for top range manufacturers and tank batteries. However, they are widespread used for traction and stand-by applications due to their life and reliability [17]. In dual energy systems, in which power capability and energy storage are distributed between two different electrochemical systems, it is possible to optimise the size, cost and performance of a gel battery to the vehicle requirements, to supply energy to the vehicle consumers during stops or when required. In the case of a hybrid configuration with a supercapacitor to provide power peaks during vehicle starts and to recuperate energy during vehicle braking, the VRLA battery should support the vehicle consumers during stops and when the supercap is charged or discharged.

A batch of batteries with a design adapted to automotive applications has been filled with a gel electrolyte, containing 6% Aerosil 200 (Degussa, fumed silica) in sulphuric acid. The battery design is included in Table 7 and the electrical performance is shown in Table 8.

The batteries were aged according to three specific cycling profiles: 60% DOD at *C*/10 rate according to IEC-896-2, 17.5% DOD at *C*/3 rate and 50% SOC and with a specific profile defined to simulate battery working conditions in a vehicle designed with the stop and start and regenerative braking functions and equipped with integrated starter generator and a supercapacitor for peak power capability.

Figs. 10 and 11 show the cycle life test results of the gel prototypes compared to those obtained with AGM UHP prototypes (type A described above). Battery life (400–450 cycles) and capacity evolution of both technologies was similar under low rate 60% DOD cycling conditions (Fig. 10), and in both cases they can be considered excellent results taking into account the positive plate thickness in the AGM batteries.

However, capacity of AGM UHP prototypes decreased steadily along the 17.5% DOD low–moderate rate cycling profile (Fig. 11), finally reaching 2975 cycles at battery failure due to voltage drop under 10 V. It is important to mention the good cycle life performance of the gel batteries: 52 units of 85 cycles each were completed (without cold cranking performance requirement, not envisaged for the application),

Table 7
The 12 V gel VRLA battery design characteristics

Dimensions, $L \times W \times H$ (mm)	175 × 80 × 174 (PP)
Nominal capacity (Ah)	18
Number of plates (+/−)	5/5
Active mass (+/−, g cell^{-1})	200/175
Separator type	Darak 2000

Table 8
Electrical testing of 12 V prototypes with gel electrolyte (6% Aerosil 200)

	Testing conditions	Results
Internal resistance (mΩ)	1 kHz, 25 °C	8.8
Capacity, C_{20} (Ah)	0.9 A, 10.5 V, 25 °C	19.3
Reserve capacity (min)	25 A, 10.5 V, 25 °C	26.4
High rate discharge (min)	90 A, 7.2 V, 25 °C	4.8
Cold cranking (s)	200 A, 7.2 V, −18 °C	44

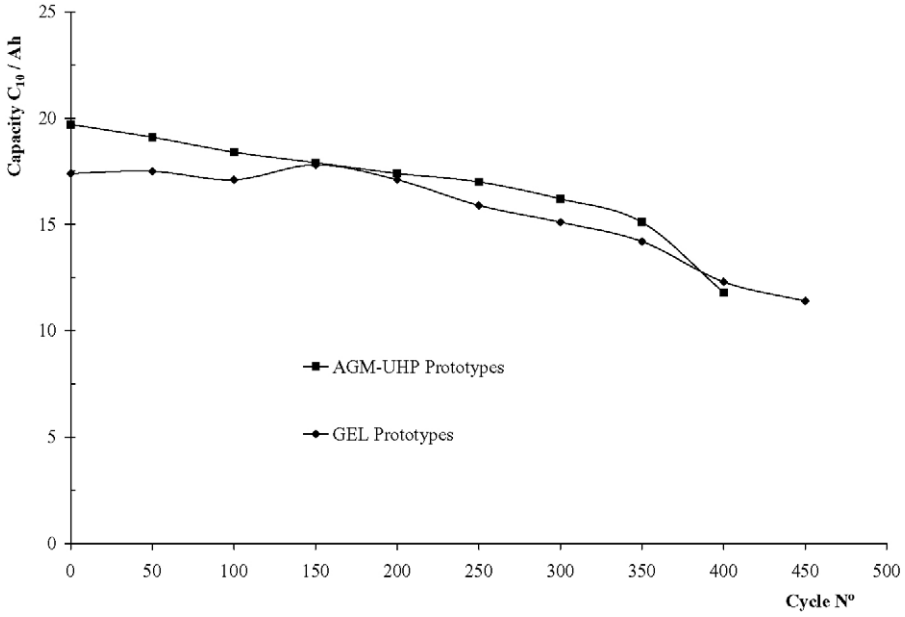

Fig. 10. Capacity evolution of AGM UHP and gel prototypes during 60% DOD cycling.

compared to the car manufacturers' demands for starter batteries (6 units for flooded batteries and 18 units for VRLA batteries).

From the driving cycle proposed by Siemens VDO Automotive within the SUPERCAR project [18], the battery working microcycle shown in Fig. 12 has been defined, and the battery was cycled at 80% SOC, and a capacity check was carried out every 10,000 microcycles, based on available drafts of EUCAR battery testing procedures for a similar application [11].

After some preliminary tests, it was detected that during constant voltage charge, current is limited when the battery reaches 16 V, and that approximately 85% of the previously discharged capacity could be recharged. Therefore, the advisable 1.03 recharge factor to maintain the state of charge of the batteries could not be reached and even a 1.0 recharge factor could not be guaranteed. In this way, it was decided to recharge the batteries at 16 V/30 A during 1 h every 500 microcycles in order to compensate the capacity loss every microcycle due to the limited charge conditions of the

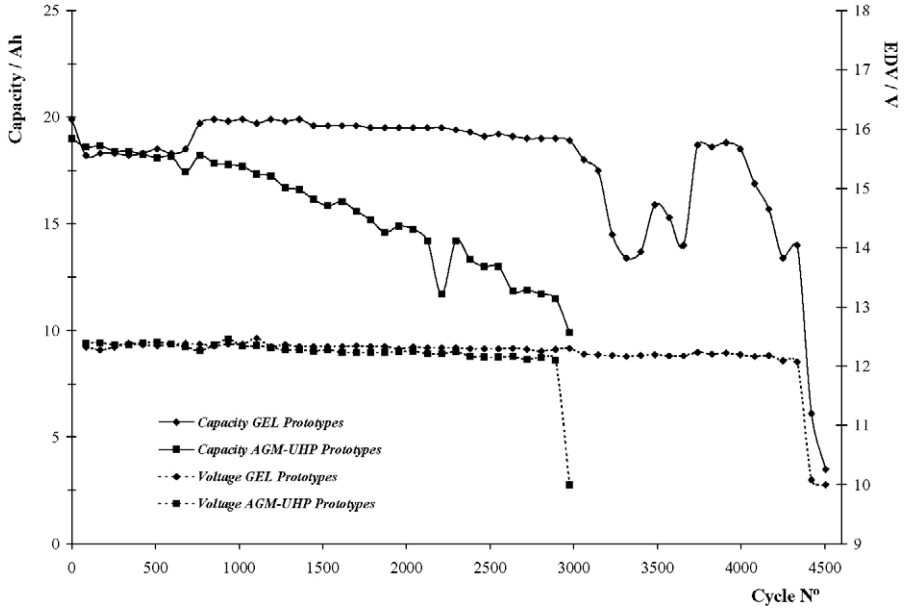

Fig. 11. Capacity and end of discharge voltage evolution of gel and AGM prototypes (17.5% DOD cycling at 50% SOC).

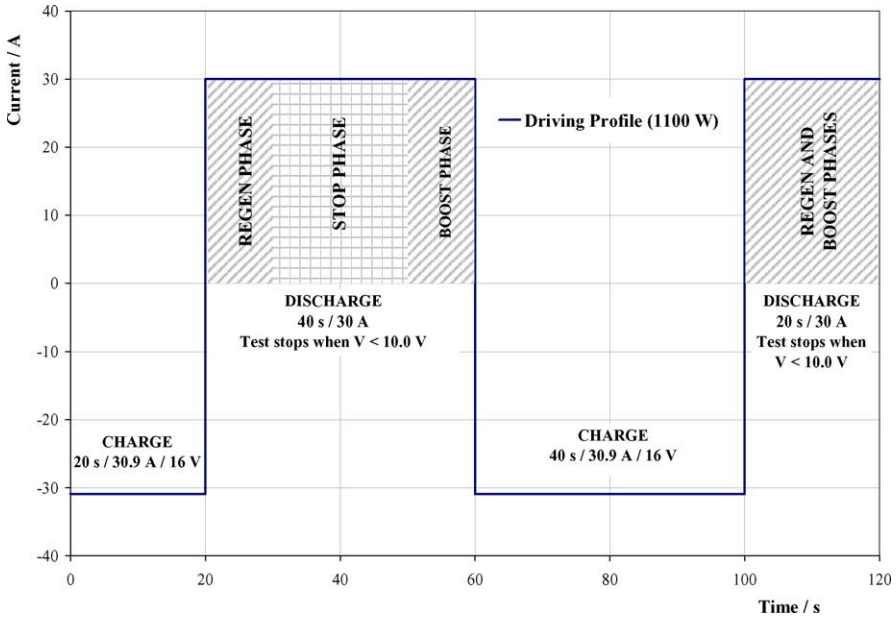

Fig. 12. Stop and start battery working profile.

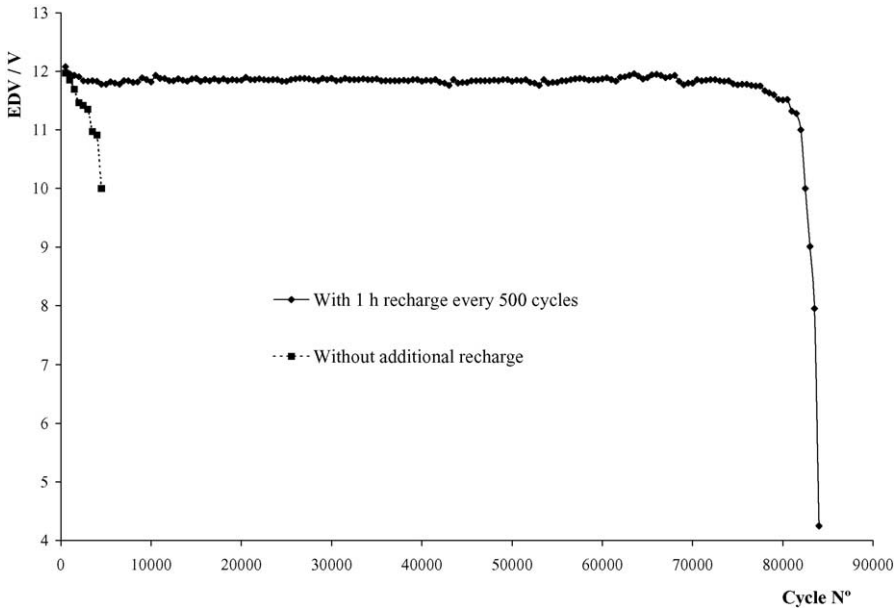

Fig. 13. End of discharge voltage (40 s pulse) of gel battery cycled according to the stop and start profile.

working profile. In the real application, this recharge simulates that every 500 km, the vehicle would run at least for 1 h in total without stopping.

Fig. 13 shows the end of discharge voltage of gel prototypes tested without the extra recharge every 500 microcycles and of the prototypes tested including such extra recharge: the former failed after around 4000 microcycles, whereas the latter completed 80,000 microcycles before failure. Records of the Ah recharged during cycling and capacity evolution showed an increased charge acceptance along battery ageing and also a significant capacity loss, even though the battery working voltage remained constant along cycling, as shown in Fig. 13.

4. Conclusions

AGM UHP prototypes show excellent performance in terms of high power capability due to the use of thin plate design and low internal resistance. However, life according to power assist profile, i.e. under high rate partial state of charge conditions, is limited due to irreversible sulphation

of negative electrodes. For this reason, negative formulations optimised to increase charge acceptance and with a special conductive additive have been tested: a lower content of Vanisperse A to increase charge acceptance and the standard carbon black used has been substituted by a higher content (1.5%) of a new type of expanded graphite. Although this formulation leads to a slightly lower discharge power capability, however, its main advantage is the increased charge acceptance along life under power assist profile: end of discharge voltage is significantly increased and thus irreversible sulphation postponed, thus doubling the PSOC life of the battery.

Under low–moderate rate partial state of charge cycling conditions, VRLA batteries with gel electrolyte show a significant life duration. Moreover, according to a specific test with a stop and start cycling profile, gel prototypes fulfilled 80,000 cycles, equivalent to 80,000 km under urban traffic conditions (stop and start).

Acknowledgements

This project is being partially funded by the European Commission, under the Energy, Environment and Sustainable Development Programme, ENERGIE Contract Nos. ENK6-CT-2000-00078 and ENK6-CT-2002-00630. The collaboration of the University of Córdoba for the structural and morphological analysis of the samples is also acknowledged.

References

[1] Kyoto Protocol, Proceedings of the Conference of the United Nations on the Climate Change, 2000.
[2] EU Green Paper “Towards a European Strategy for the Security of Energy Supply”, November 2000.
[3] Well-to-wheels analysis of future automotive fuels and powertrains in the European context, EUCAR, CONCAWE, JRC, November 2003.
[4] D. Carney, Automotive Eng. Int. (2004) 50–56.
[5] D. Linden, T.B. Reddy, Handbook of Batteries, 3rd ed., McGraw-Hill, New York, 2002, pp. 22.1–22.24.
[6] R. Knorr, A. Schwake, M. Soria, H. García, M. Reimerink, D. Macerata, M. Ullrich, Proceedings of the ELEDrive Transportation Conference, Estoril, Portugal, March, 2004.
[7] M.L. Soria, J. Valenciano, A. Ojeda, G. Raybaut, K. Ihmels, J. Deiters, N. Clement, J. Morales, L. Sánchez, J. Power Sources 116 (2003) 61–72.
[8] M.L. Soria, J. Valenciano, A. Ojeda, J. Power Sources 136 (2004) 376–382;
M.L. Soria, J. Valenciano, A. Ojeda, in: A. Attewell (Ed.), Proceedings of the 23rd International Power Sources Symposium, Amsterdam, September 2003, Power Sources 19 (2003).
[9] J. Valenciano, F. Trinidad, J. Sáinz, Proceedings of the 8th ALABC Members and Contractors Conference, Nice, June, 2003.
[10] J. Valenciano, F. Trinidad, Proceedings of the 2nd European Conference on Alternative Energy Sources for Automobiles, Poitiers, France, April, 2004.
[11] EUCAR Traction Battery Working Group: (a) Specification of test procedures for hybrid electric vehicle traction batteries, September 1998; (b) Specification of test procedures for energy storage of 42 V-vehicle applications, August 2003.
[12] K. Peters, in: D.A.J. Rand, P.T. Moseley, J. Garche, C.D. Parker (Eds.), Valve Regulated Lead-acid Batteries, Elsevier, Amsterdam, 2004, p. 137.
[13] L.T. Lam, N.P. Haigh, C.G. Phyland, A.J. Urban, J. Power Sources 133 (2004) 126–134.
[14] M.L. Soria, J. Sáinz, J. Valenciano, Proceedings of the STORE Conference on Storage for Renewable Energies, Aix-en-Provence, France, October, 2003.
[15] R. Wagner, J. Power Sources 53 (1995) 153–162.
[16] M. Ohnishi, K. Ito, S. Yuasa, N. Fujioka, T. Asahina, S. Hmada, T. Eto, Proceedings of the 3rd International Advanced Automotive Battery Conference, Nice, France, June, 2003.
[17] R. Wagner, in: D.A.J. Rand, P.T. Moseley, J. Garche, C.D. Parker (Eds.), Valve-regulated Lead-acid Batteries, Elsevier, Amsterdam, 2004, p. 447.
[18] Improved energy supply for the integrated starter generator with double layer capacitor and energy battery for cars with 42 V (SUPERCAR), ENERGIE Contract No. ENK6-CT-2002-00630.